Quantum simulation of ^{3}He impurities and of ^{4}He interstitials in solid ^{4}He

Keola Wierschem[1] and Efstratios Manousakis[1,2]
[1]*Department of Physics, Florida State University, Tallahassee, Florida 32306-4350, USA*
[2]*Department of Physics, University of Athens, Penipistimiopolis, Zografos, 157 84 Athens, Greece*
(Received 15 September 2010; published 16 November 2010)

We have studied the role of an atomic ^{3}He impurity and an interstitial ^{4}He atom in two-dimensional (2D) and three-dimensional (3D) solid ^{4}He using path-integral Monte Carlo simulation. We find that when a substitutional ^{3}He impurity is introduced, the impurity becomes localized and occupies an ideal lattice site. When an interstitial ^{3}He impurity is introduced in the ^{4}He solid, we find that the impurity becomes localized at a substitutional position and, thus, promotes the extra ^{4}He atom to the interstitial space. As a consequence we find that the one-body density matrix (OBDM) and the superfluid fraction, for the case of a ^{4}He solid with an interstitial impurity, are very similar to those calculated for a ^{4}He solid with a ^{4}He interstitial atom. Namely, while the off-diagonal OBDM approaches zero exponentially with increasing particle displacement for the "pure" solid, an interstitial ^{4}He atom or a ^{3}He impurity appear to enhance it at long distances. Finally, the effective mass of the ^{3}He impurity quasiparticle in 2D and 3D crystalline ^{4}He is estimated.

DOI: 10.1103/PhysRevB.82.184524 PACS number(s): 05.30.Jp, 67.80.bd, 67.80.dj

I. INTRODUCTION

The torsional oscillator experiments of Kim and Chan,[1] where at low temperature a drop in the moment of inertia is observed, have motivated a number of computational studies[2–9] of solid ^{4}He as well as various theoretical proposals[10–12] to explain the observation. Additionally, the annealing and quenching torsional oscillator experiments of Ritter and Reppy [13] have shown the important role of defects in the outcomes of these experiments.

There is evidence of a very strong dependence of the superfluid response on the ^{3}He impurity concentration[14] as well as other well known facts[15] about the role of impurities in solid ^{4}He.[16–18] Proposals for the possible role of ^{3}He impurities in solid ^{4}He have a long history and date back in the late 60s (Ref. 19) and 70s.[20,21] In addition, there are several experimental studies of the NMR relaxation of such impurities in solid helium.[22] It is, therefore, of great interest to study the role of impurities in solid ^{4}He. Boninsegni *et al.*[6] have carried out a path-integral Monte Carlo (PIMC) simulation of three-dimensional (3D) solid ^{4}He using the worm algorithm and found that vacancies phase separate. Pollet *et al.*[7] and Boninsegni *et al.*[8] have also used the above PIMC technique to show that grain boundaries in solid ^{4}He and screw dislocations lead to superfluidity. In addition, using the same method Pollet *et al.*[9] have shown that the gap to create vacancies closes by applying a moderate stress.

In the present paper, motivated by the recent experimental and theoretical activity on the possible role of the ^{3}He impurities in solid ^{4}He, we study the role of a ^{3}He impurity and of an interstitial ^{4}He atom in two-dimensional (2D) and 3D solid ^{4}He using PIMC simulation. In addition to the motivation generated by the previous discussed experimental activity, this problem is of interest in its own right because it is not really known what happens locally when one injects a ^{3}He atom in 2D or 3D solid ^{4}He, and this can be studied by quantum simulation. In particular, we use the worm algorithm[5] to simulate the 2D and 3D solid helium in the presence of such crystalline defects. We present results of the radial distribution functions and off-diagonal one-body density matrix (OBDM) for the following cases. (a) Pure solid ^{4}He at somewhat above but near the liquid-solid melting density (ρ=0.026 Å^{-3} for 3D and σ=0.070 Å^{-2} for the pure 2D case[23–25]). (b) A single substitutional ^{3}He impurity in solid ^{4}He. (c) An interstitial ^{4}He atom (defect). This atom is identical to the other ^{4}He atoms and, therefore, it participates in permutation cycles. (d) An interstitial ^{3}He impurity in solid ^{4}He.

We find that an initial interstitial impurity quickly relaxes to a regular lattice site of the ^{4}He solid by creating an interstitial ^{4}He atom as was proposed in Ref. 11. Furthermore, we find that introducing such interstitial impurities in ^{4}He solid greatly enhances the long-distance part of the off-diagonal OBDM. This enhancement as well as the calculated superfluid response is comparable to that of interstitial ^{4}He atomic defects. It is quite possible that at a finite density interstitial ^{4}He atoms phase separate as do vacancies.[6] In such case the enhancement of the OBDM at long distances and of the superfluid density, due to a single interstitial ^{3}He or ^{4}He atom found in the present paper, may disappear when a finite density of such impurities or interstitials is introduced. However, interstitial atoms or impurity atoms can bind to already existing defects, such as dislocations or disclinations (especially in 2D) and this tendency for phase separation may be avoided. In general, it is of great value to know what happens *locally* in the 2D and in the 3D crystalline ^{4}He when a ^{3}He impurity or an interstitial ^{4}He atom is introduced.

The paper is organized as follows: in Sec. II we briefly describe the PIMC method used to study this system. In Sec. III, we present and discuss the pair-distribution functions for the case of a 2D and 3D solid with and without the introduction of a ^{3}He impurity and ^{4}He interstitial atom. The energetics of creating such atomic defects in the 2D and 3D solids as well as the calculation of the effective mass of ^{3}He impurity in solid ^{4}He is discussed in Sec. IV. In Sec. V we present the results for the one-body density matrix, the superfluid density and a histogram of the number of particles involved in the same permutation cycle for the cases (a)–(d)

above for 2D and 3D solid helium. Finally, the main findings as well as the limitations of the present work are discussed in Sec. VI.

II. SIMULATION DETAILS

Using an approximation for the density matrix that is accurate to fourth order[26] in τ, we use 320 time slices to reach a simulation temperature of 1 K. We have collected data from 2500 continuous iterations for our simulations in 2D, and ~1000 continuous iterations for our simulations in 3D. Each iteration consists of 500 Monte Carlo moves. All data presented in this paper were obtained at a simulation temperature of 1 K, unless otherwise stated.

All simulated atoms considered in our present studies are isotopes of helium and therefore interact via the same potential. We use the Aziz[27] potential to model both the ^{4}He-^{4}He interaction and the ^{3}He-^{4}He interaction. With the exception of the ^{3}He impurity atom the rest are all ^{4}He atoms which will be treated appropriately to simulate their bosonic nature. The impurity atom is distinguishable from the "background" ^{4}He atoms.

Our simulation cell is designed to accommodate either a 2D 56-site triangular lattice that is very nearly square (25.86 Å × 25.60 Å), or a 3D 180-site hexagonal close-packed lattice (18.35 Å × 19.07 Å × 17.98 Å). In both cases of the 2D and 3D lattices we have used periodic boundary conditions. The density of lattice sites is fixed at 0.0846 Å^{-2} (2D) and 0.0286 Å^{-3} (3D). We will use the term *pure solid* for the case where there is exactly one ^{4}He atom per lattice site. The term *substitutional solid* will be used when a single ^{4}He atom is removed from the pure solid and is replaced with an impurity atom. Additionally, the term *interstitial solid* will be used when a single atom (either ^{4}He or an impurity) is added to the pure solid.

III. DISTRIBUTION FUNCTIONS

In this section we present our results for the various combinations of pair-distribution functions. Besides the fact that these quantities are directly related (via Fourier transforms) to the static structure factor which can be accessible to experiments, they will also help us draw conclusions about the role of ^{3}He impurities and interstitials locally in the 2D and 3D solid.

A. Two-dimensional solid ^{4}He

How does the impurity atom affect the pair-distribution function g_{44} of the ^{4}He atoms of the underlying solid? We find that when a substitutional impurity is introduced it becomes localized and occupies an ideal lattice position with its own zero-point motion determined by its different mass. In Fig. 1 we present the calculated $g_{44}(r)$ radial distribution for pairs of ^{4}He atoms for the four different case systems studied: (a) pure solid ^{4}He (dashed line), (b) the ^{4}He solid with a substitutional ^{3}He impurity (also dashed line), (c) the ^{4}He solid with an interstitial ^{4}He defect (solid line), and (d) the ^{4}He solid with an interstitial ^{3}He impurity (also solid line). Within the accuracy of our results we cannot discern

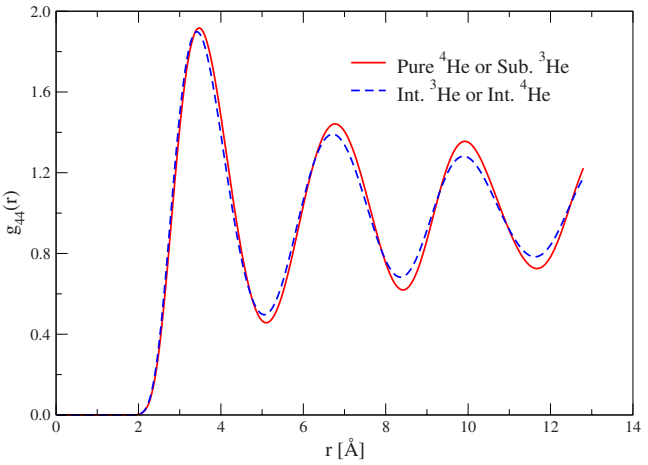

FIG. 1. (Color online) Here we show the radial distribution function, $g_{44}(r)$, for pairs of ^{4}He atoms in two dimensions. The organizational structure of the ^{4}He atoms does not change in the presence of a substitutional impurity. However, when an interstitial defect or impurity is present, we can see that $g_{44}(r)$ becomes less peaked at the nearest-neighbor distance lattice positions.

any difference in the g_{44} distribution function for the cases of the pure solid and the substitutional impurities. When an interstitial impurity is present in the ^{4}He solid, we find that the impurity becomes localized at a substitutional position, thereby promoting the extra ^{4}He atom to the interstitial band. This is shown by the snapshot space-time configuration shown in Fig. 2. Notice that while the initial configuration has an interstitial ^{3}He impurity, in the configuration obtained after thermalization (shown in Fig. 2) the ^{3}He becomes substitutional by promoting an interstitial ^{4}He atom. Namely, in the equilibrium configuration, shown in Fig. 2, the ^{3}He atom, in our lattice with periodic boundary conditions, is located in a regular triangular lattice position surrounded by six ^{4}He atoms. In addition, a ^{4}He atom has been promoted to the

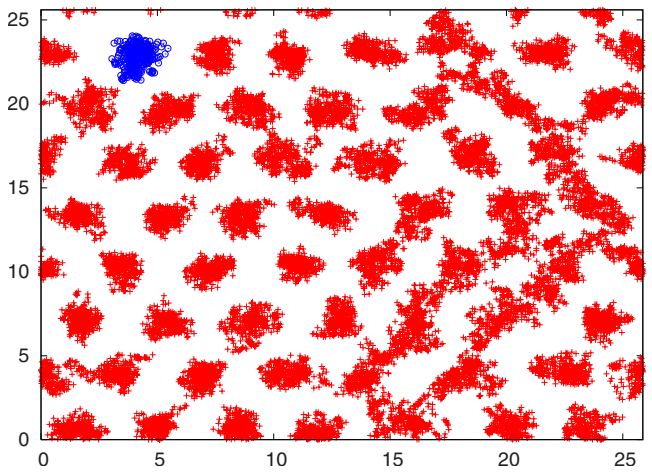

FIG. 2. (Color online) A snapshot of a space-time configuration for the 2D triangular solid, after thermalization, and starting from a configuration with an interstitial ^{3}He atom. Each atom's trajectory in imaginary time appears as fractal covering a finite size spot. The crosses (red in the online version) and the circles (blue in the online version) are the ^{4}He atoms and the ^{3}He impurity atom.

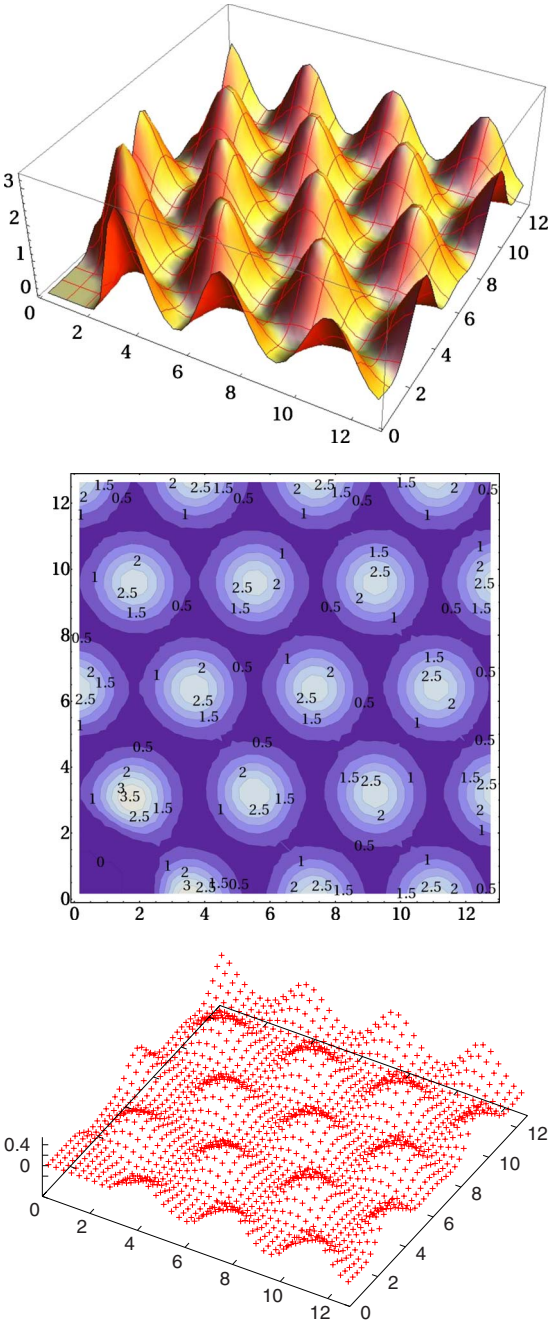

FIG. 3. (Color online) Top: the pair-distribution function $g_{44}(x,y)$ for pure 2D solid ^{4}He. Middle: contour plot of the distribution function for pairs of ^{4}He atoms, $g_{44}(x,y)$ in the pure solid. Bottom: the difference δg_{44} between g_{44} of the pure (solid) and that of the solid with interstitial impurity.

interstitial space which creates larger density fluctuations in the crystalline arrangement in some parts of the system. As a consequence of this fact $g_{44}(r)$, in Fig. 1, is less peaked at the lattice positions. In Fig. 3 (top) the calculated pair-distribution function $g_{44}(x,y)$ for pure 2D solid ^{4}He is shown and in Fig. 3 (middle) we present the contour plot of the same $g_{44}(x,y)$. This function is nearly identical for the substitutional solid (which is not shown, as it looks exactly alike). This implies that the introduced substitutional impurity becomes localized and it only affects its neighboring

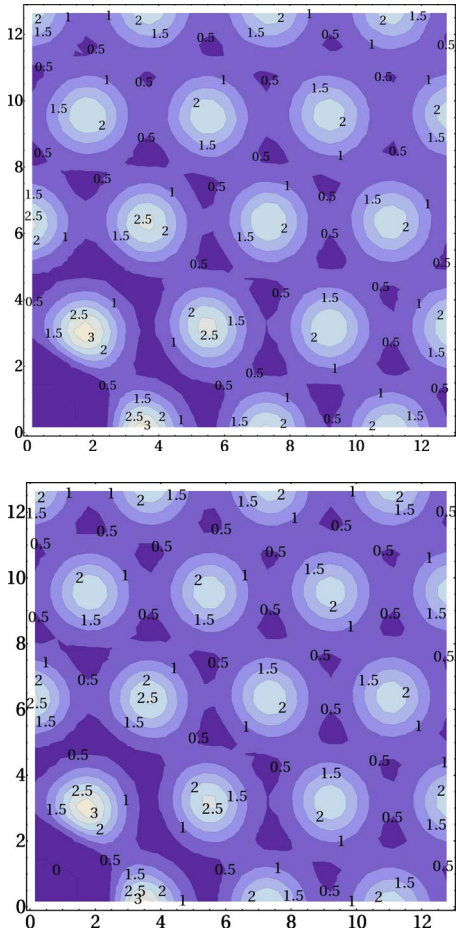

FIG. 4. (Color online) Top panel: contour plot $g_{44}(x,y)$ for the interstitial solid. This function is independent of the type of defect or impurity. Bottom panel: contour plot of the distribution function $g_{34}(x,y)$ for the same interstitial solid.

atoms. In the case of an interstitial impurity the difference in the g_{44} distribution function, as discussed above and shown in Fig. 1 and Fig. 3 (bottom), is significant because the added impurity takes the position of a ^{4}He atom and, thus, there is an extra ^{4}He atom that necessarily becomes interstitial. In the bottom panel of Fig. 3 we plot $\delta g_{44}(x,y)$, the difference between $g_{44}(x,y)$ of the pure solid and the solid with a single interstitial impurity. Notice that the extra atom is truly interstitial since the g_{44} is reduced by an amount in the neighborhood of the ideal lattice positions and enhanced in the interstitial space by the same amount. It was verified through integration in the enhanced regions (or the reduced regions) finding exactly one extra ^{4}He atom in the interstitial regions.

Our finding that the interstitial impurity becomes localized at regular lattice sites can be further illustrated by comparing the contour plots of the $g_{44}(x,y)$ and $g_{34}(x,y)$ for the case where we have a ^{4}He solid with an interstitial impurity. In the top panel of Fig. 4, we present the contour plot of the distribution function $g_{44}(x,y)$ for the case of a ^{4}He solid with an interstitial impurity. Within the accuracy of the discretization of the probability density of the contour plot this function is independent of the type of defect or impurity. In the lower panel is the distribution function $g_{34}(x,y)$ for pairs

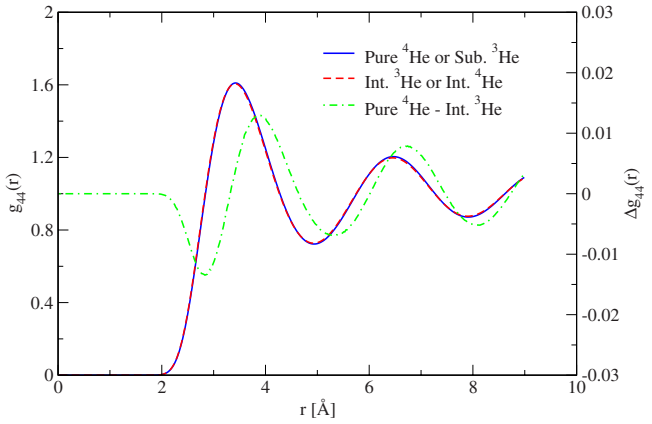

FIG. 5. (Color online) The radial distribution function for pairs of ^{4}He atoms in the three-dimensional HCP lattice simulation cell, $g_{44}(r)$. The organizational structure of the ^{4}He atoms does not change in the presence of a substitutional impurity. However, when an interstitial defect or impurity is present, by looking at $\Delta g_{44}(r)$ (scale on the right) we can see that $g_{44}(r)$ becomes less peaked at the nearest-neighbor distance lattice positions.

consisting of the impurity atom and one ^{4}He atom. Because the contour plots for both $g_{34}(x,y)$ and $g_{44}(x,y)$ are identical in shape and in form, we may surmise that the impurity atoms are located at lattice sites.

B. Three-dimensional solid ^{4}He

In Fig. 5 we show $g_{44}(r)$ for the 3D system. As in 2D, we find that the pure solid and the substitutional solid are nearly identical in structure, as are the two interstitial solids. Also shown is the difference, $\Delta g_{44}(r)$, between $g_{44}(r)$ the pure solid and the interstitial solid. As expected, $g_{44}(r)$ for both interstitial solids is less peaked at lattice positions compared to the pure and substitutional solids. This indicates that the ^{4}He interstitial solid really does have a ^{4}He atom in the interstitial space, and also that the interstitial ^{3}He solid has relaxed into a space where the ^{3}He interstitial atom has become substitutional, and in doing so promoted a ^{4}He atom to the interstitial band.

IV. ENERGETICS OF IMPURITY AND INTERSTITIAL

If a ^{3}He atom, initially placed in the interstitial region of a triangular solid of ^{4}He atoms, relaxes onto a lattice site by promotion of a ^{4}He atom to the interstitial space, this should be seen in the energy values of the simulated atoms. The potential energy of a ^{3}He atom in the substitutional and interstitial ^{3}He solids as a function of the Monte Carlo iteration shows that there is a short relaxation time for the interstitial solid, as the ^{3}He atom relaxes onto the lattice. After that short relaxation time scale, the potential energy of a ^{3}He atom in both systems is almost the same. After several hundreds of iterations, small bumps can be seen in the energy of the (initially) interstitial ^{3}He atom. During these bumps the ^{3}He atom is no longer at an equilibrium lattice position but rather at what appears to be a possible edge dislocation. This is not entirely unexpected, as a ^{3}He atom in solid ^{4}He exhibits a high rate of diffusion. Such "blips" in the energy of the ^{3}He in the interstitial solid occur occasionally throughout our simulation but account for no more than 5% of configurations.

TABLE I. Excitation energy of an interstitial ^{4}He atom, as calculated by the difference in energy between (1) the pure solid and the interstitial ^{4}He solid and (2) the substitutional solid and the interstitial ^{3}He solid.

Energy difference	2D	3D
Int. ^{4}He−pure ^{4}He	50.27 ± 0.54 K	22.4 ± 1.3 K
Int. ^{3}He−sub. ^{3}He	50.41 ± 0.55 K	24.1 ± 1.2 K

In Table I we show the activation energy of an interstitial ^{4}He atomic defect. This is calculated by subtracting the total energy of the pure solid from the total energy of the interstitial ^{4}He solid. If the interstitial ^{3}He solid is actually the substitutional solid with an added interstitial ^{4}He atom, as we propose it is based on the distribution functions above, then the activation energy can also be calculated by subtracting the total energy of the substitutional solid from the total energy of the interstitial ^{3}He solid. We find that both methods give activation energies in agreement with one another. Notice that the value of the activation energy for an interstitial in the 3D solid compares well with that reported by Boninsegni *et al.*[6]

We have also estimated the effective mass of the ^{3}He impurity in solid 2D and 3D ^{4}He using our data on the imaginary time diffusion following Ref. 28. Namely, we approximate the low-energy (which dominates the long time evolution) impurity quasiparticle spectrum by the dispersion near the Γ point of the Brillouin zone of both the triangular 2D solid and of the hexagonal closed packed 3D lattice

$$E(k) = \Delta + \frac{\hbar^2 k^2}{2m^*}. \tag{1}$$

It is straightforward to carry out the imaginary-time evolution for this spectrum and to calculate the average of $[\mathbf{r}(0) - \mathbf{r}(\tau)]^2$, where $\mathbf{r}(\tau)$ is the impurity coordinate in imaginary time. When we use the expression given by Eq. (1), we find that the quantity,

$$R(\tau) = \frac{\langle [\mathbf{r}(0) - \mathbf{r}(\tau)]^2 \rangle}{2d\lambda} \frac{\beta}{\tau(\beta - \tau)}, \tag{2}$$

where $\lambda = \hbar^2/(2m)$ and d is the dimensionality, is a constant independent of τ and it is equal to m/m^*. In practice, however, $R(\tau)$ is expected to be a function of τ, which defines a quantity $m/m^*(\tau)$, i.e., an imaginary-time-dependent effective mass which for short time scales (high-energy scales) it should be equal to 1, and at long time scales it should give the low-energy quasiparticle effective mass (see Fig. 6). Therefore, we can define a temperature-dependent effective mass at temperature T as

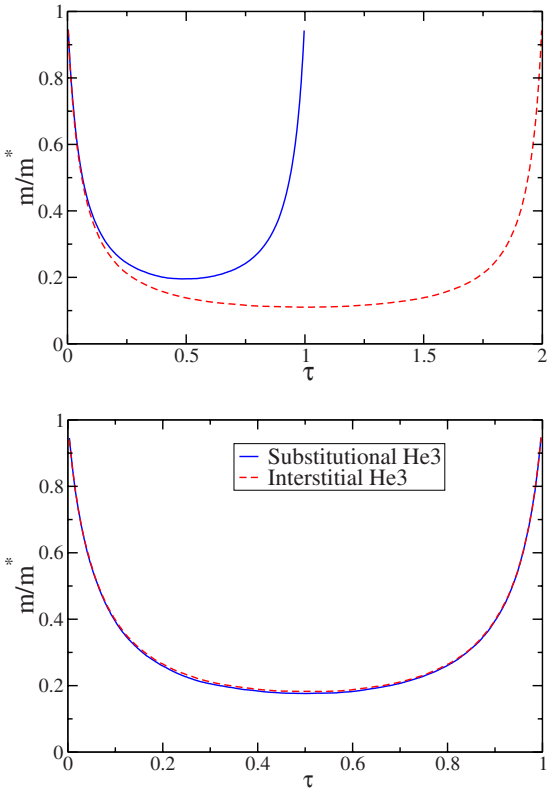

FIG. 6. (Color online) Top: the ratio m/m^* as a function of τ for 2D interstitial impurity and $T=1$ K (Solid line) and $T=0.5$ K (dashed line). Bottom: the ratio m/m^* as a function of τ for 3D and $T=1$ K for substitutional and interstitial ^{3}He impurities.

$$\frac{m}{m^*} = R(\tau)|_{\tau=\beta/2}, \tag{3}$$

as the mass which controls the longest possible imaginary-time diffusion which is $\tau_{\max}=\beta/2$. Clearly, this is meaningful when the correlation function given by Eq. (2) above becomes flat near $\tau=\beta/2$ (see Fig. 6).

In Fig. 6 we plot the right-hand side of Eq. (2) as calculated from our simulation for the 2D [Fig. 6 (top)] and 3D [Fig. 6 (bottom)] case. We find that in the 2D case the effective mass ratio of the ^{3}He interstitial impurity at $T=1$ K is 5.10 ± 0.02 while at $T=0.5$ K it increases to 9.06 ± 0.04. In the 3D case we have available results only for $T=1$ K, where the substitutional and the interstitial impurity masses are found to be 5.67 ± 0.03 and 5.47 ± 0.04, respectively.

V. OFF-DIAGONAL ONE-BODY DENSITY MATRIX

In Fig. 7 we compare the one-body density matrix $n(r)$ for (a) defect-free solid ^{4}He (solid line), (b) solid ^{4}He with a substitutional ^{3}He impurity (dotted line), (c) solid ^{4}He with an interstitial ^{4}He defect (long-dashed line), (d) solid ^{4}He with an interstitial ^{3}He impurity (dashed line). Notice that the substitutional ^{3}He impurity and the pure solid have similar one-body density matrices. On the contrary, a ^{4}He solid with interstitial ^{3}He impurity and a ^{4}He solid with interstitial ^{4}He atoms have one-body density matrices which are significantly enhanced at long distances. This result agrees with the fact that winding numbers (and hence superflow) are observed in the interstitial solid (see Table II). Notice that these superfluid fractions are very high considering that the simulation was carried out at 1 K. The reason for these high superfluid fractions is finite-size effects. These results for the superfluid fraction are presented in order to make the case that an interstitial impurity has a very similar effect on the superfluid fraction and OBDM as an interstitial ^{4}He atom.

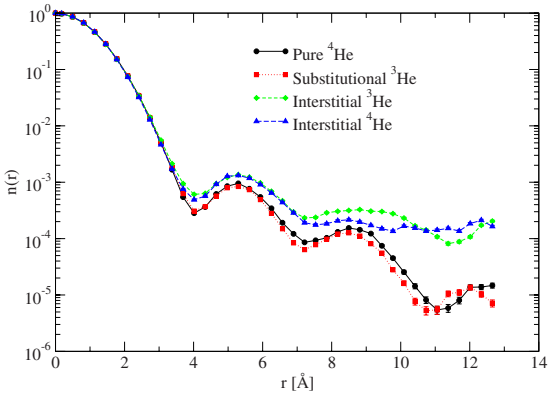

FIG. 7. (Color online) The one-body density matrix, $n(r)$. Although no difference is observed between the pure solid and the substitutional solid, the interstitial solid clearly shows a significant enhancement of $n(r)$ quantity.

In Fig. 8 we compare the one-body density matrix for the 3D results. As in 2D, both the pure solid and the substitutional solid show exponential decay of $n(r)$. Although the enhancement of $n(r)$ at large distance is not obvious for the interstitial ^{3}He solid, it is very clear for the interstitial ^{4}He solid. This may be due to a shorter MC run as compared to the 2D data. In any case, once again both interstitial solids display superfluidity while the pure and substitutional solids do not (see Table II). For comparison we have included the $n(r)$ for the case of ^{4}He solid with vacancies taken from the work of Galli *et al.*[29] Notice that the interstitial solid and the solid with vacancies have comparable $n(r)$ for large r.

In Fig. 9 we present a histogram of cycles (i.e., how often in the simulation we encounter cycles of exchanges involving a given number of particles). Notice that in both 2D and 3D case, the pure solid and the ^{3}He substitutional solid has only one or two particle permutation cycles, while when an interstitial ^{3}He or ^{4}He atom is introduced, it gives rise to permutations involving up to a ten-atom chain, which is as long as the longest possible distance in our lattice. This indicates that the result may not be a finite-size effect.

TABLE II. Supersolid fraction, ρ_s/ρ, in the presence of an interstitial atom. No global permutations were observed for the perfect lattice and the substitutional impurity.

Case	2D	3D
Interstitial ^{3}He	0.021(7)	0.007(4)
Interstitial ^{4}He	0.011(6)	0.012(5)

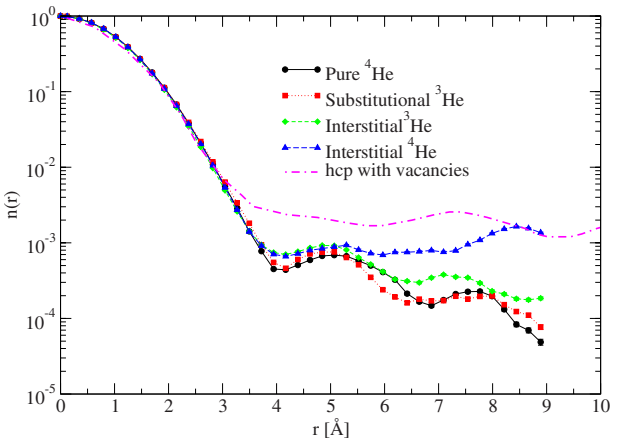

FIG. 8. (Color online) The one-body density matrix, $n(r)$, of the 180-site hcp system in three dimensions. Although no difference is observed between the pure solid and the substitutional solid, the interstitial solid clearly shows a significant enhancement of $n(r)$. For comparison to the case of vacancies we have included the line labeled "hcp with vacancies" which is taken from the paper by Galli *et al.* (Ref. 29) and it corresponds to an hcp density of 0.029 $Å^{-3}$ with 0.558% vacancies.

VI. DISCUSSION

One of the main conclusions of the present paper is that the added interstitial impurity in both 2D and 3D ^{4}He becomes substitutional by creating an interstitial ^{4}He defect; we believe that this result is firm and it is not subject to finite-size effects. Furthermore, we find that the effective mass of a ^{3}He impurity atom in both 2D and 3D solid ^{4}He is large at $T=1$ K ($m^*/m \sim 5$) and at a lower temperature of 500 mK in 2D it becomes even larger ($m^*/m \sim 9$).

In addition, we find that the above-mentioned effect (i.e., the promotion of a ^{4}He atom to the interstitial band by the impurity) gives rise to a nonzero superfluid response and a significant enhancement of the OBDM at long distances. This suggests that, provided that this effect persists when a finite density of ^{3}He impurities is present and, provided that such a metastable state can be created and maintained, ^{4}He solid with such impurities should be a supersolid. However, this cannot be established by the present calculation done for a single impurity in a pure ^{4}He solid and it depends on a number of other factors. For example, while we have clearly demonstrated that a single ^{3}He impurity acts as a donor of ^{4}He atoms to the interstitial (conduction) band, the fate of these freed bosonic "carriers" is not certain when there is a finite density of ^{3}He impurities. In this case the created interstitial ^{4}He atoms can phase separate in a similar way as vacancies do,[6] or they may bind to existing defects, such as, dislocations, domain walls, or grain boundaries or even remain free. It is not clear that such interstitial defects exist in the ^{4}He solid caused by ^{3}He or other impurities. This is an issue which could depend on the process of the crystal growth.[16–18]

A 2D ^{4}He solid only exists as films on substrates, such as on graphite. The phase diagrams of first, second, third, and fourth layer of ^{4}He on graphite, as a function coverage, has been studied by PIMC simulation.[25,30] The role of substrate

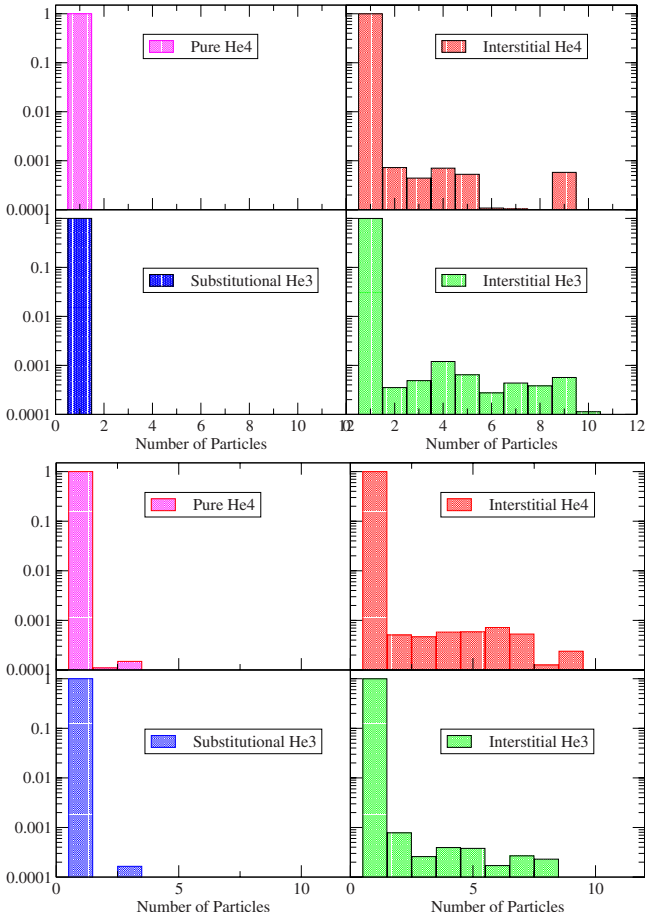

FIG. 9. (Color online) Histogram of relative frequency of accepted particle permutations for various number of particles in 2D (top figure) and 3D (bottom figure).

corrugations, which is missing from the present simulation of the ideal 2D ^{4}He, is important and the interplay of these substrate potential corrugations with the helium-helium interaction gives rise to a wealth of interesting phases.[25,30] It is quite possible, however, that the main conclusion of the present paper, that introducing an interstitial ^{3}He impurity in solid ^{4}He leads to the promotion of a ^{4}He atom to an interstitial position while the ^{3}He impurity becomes substitutional, may remain valid even in the case of substrate corrugations.

The superfluid response which was calculated at 1 K and is given in Table II is very large considering the fact that the calculation was done at such a high temperature. This is a finite-size effect but at a much lower temperature the superfluid response is expected to be greater. A calculation of the superfluid density at a significantly lower temperature requires much larger computational time scales in order to be able to accurately sample it. In the 3D case, the zero-temperature condensate fraction obtained as the asymptotic value (infinite distance value) of the off-diagonal OBDM at zero temperature, is much smaller by at least one order of magnitude (as seen from Fig. 8). Therefore, as is well known, there is a large factor relating the superfluid response and the actual condensate fraction. It is clear that introducing just a single impurity and taking the infinite volume limit (or

infinite area limit in 2D), the superfluid density and the condensate fraction should vanish. It is interesting, however, the fact that the ratio x_s/x of the superfluid fraction $x_s=\rho_s/\rho$ to the impurity fraction x (the impurity fraction is $1/N$, where N is the total number of ^{4}He atoms considered) is a number of order unity. Futhermore, the ratio n_0/x of the condensate fraction $n_0=n(r\rightarrow\infty)$ to the impurity fraction for the 3D interstitial solid case is of order 0.1. We remind the reader that in strongly interacting Bose quantum fluids such as liquid ^{4}He, the zero-temperature condensate fraction[31] is only 0.1.

Our reported results on the off-diagonal OBDM and superfluid density are very interesting, however, one cannot draw firm definite conclusions because of (a) finite-size effects and (b) they refer to the case of a single ^{3}He impurity or single ^{4}He interstitial.

ACKNOWLEDGMENTS

We want to thank Massimo Boninsegni for useful discussions and for his help with applying the worm algorithm to this problem. This work was partially supported by a NASA under Grant No. NAG3-2867.

[1] E. Kim and M. H. W. Chan, Nature (London) **427**, 225 (2004); Science **305**, 1941 (2004).
[2] N. Prokof'ev and B. Svistunov, Phys. Rev. Lett. **94**, 155302 (2005); E. Burovski, E. Kozik, A. Kuklov, N. Prokof'ev, and B. Svistunov, *ibid.* **94**, 165301 (2005).
[3] D. M. Ceperley and B. Bernu, Phys. Rev. Lett. **93**, 155303 (2004); B. K. Clark and D. M. Ceperley, *ibid.* **96**, 105302 (2006); M. Boninsegni, N. Prokof'ev, and B. Svistunov, *ibid.* **96**, 105301 (2006).
[4] M. Boninsegni and N. V. Prokof'ev, Phys. Rev. Lett. **95**, 237204 (2005).
[5] M. Boninsegni, N. V. Prokof'ev, and B. V. Svistunov, Phys. Rev. Lett. **96**, 070601 (2006); Phys. Rev. E **74**, 036701 (2006).
[6] M. Boninsegni, A. B. Kuklov, L. Pollet, N. V. Prokof'ev, B. V. Svitsunov, and M. Troyer, Phys. Rev. Lett. **97**, 080401 (2006).
[7] L. Pollet, M. Boninsegni, A. B. Kuklov, N. V. Prokof'ev, B. V. Svitsunov, and M. Troyer, Phys. Rev. Lett. **98**, 135301 (2007).
[8] M. Boninsegni, A. B. Kuklov, L. Pollet, N. V. Prokof'ev, B. V. Svitsunov, and M. Troyer, Phys. Rev. Lett. **99**, 035301 (2007).
[9] L. Pollet, M. Boninsegni, A. B. Kuklov, N. V. Prokof'ev, B. V. Svitsunov, and M. Troyer, Phys. Rev. Lett. **101**, 097202 (2008).
[10] A. T. Dorsey, P. M. Goldbart, and J. Toner, Phys. Rev. Lett. **96**, 055301 (2006).
[11] E. Manousakis, EPL **78**, 36002 (2007).
[12] J. Toner, Phys. Rev. Lett. **100**, 035302 (2008).
[13] A. S. C. Rittner and J. D. Reppy, Phys. Rev. Lett. **97**, 165301 (2006); **98**, 175302 (2007).
[14] E. Kim and M. H. W. Chan, J. Low Temp. Phys. **138**, 859 (2005); E. Kim, J. S. Xia, J. T. West, X. Lin, A. C. Clark, and M. H. W. Chan, Phys. Rev. Lett. **100**, 065301 (2008).
[15] P.-C. Ho, I. P. Bindloss, and J. M. Goodkind, J. Low Temp. Phys. **109**, 409 (1997).
[16] A. Smith, V. A. Maidanov, E. Y. Rudavskii, V. N. Grigor'ev, V. V. Slezov, M. Poole, J. Saunders, and B. Cowan, Phys. Rev. B **67**, 245314 (2003).
[17] E. Rudavskii, A. Ganshin, V. N. Grigor'ev, V. Maidanov, N. Omelaenko, A. Penzev, and A. Rybalko, J. Low Temp. Phys. **121**, 713 (2000).
[18] A. Ganshin, V. Grigor'ev, V. Maidanov, N. Omelaenko, A. Penzev, E. Rudavskii, and A. Rybalko, J. Low Temp. Phys. **116**, 349 (1999).
[19] A. F. Andreev and I. M. Lifshitz, Sov. Phys. JETP **29**, 1107 (1969); A. F. Andreev and A. E. Meierovich, *ibid.* **40**, 776 (1974).
[20] A. F. Andreev, Sov. Phys. JETP **41**, 1170 (1976).
[21] Y. Kagan, *Defects in Insulating Crystals* (Springer-Verlag, Berlin, 1981), p. 17; Y. Kagan and L. A. Maksimov, Sov. Phys. JETP **60**, 201 (1984).
[22] R. A. Guyer, R. C. Richardson, and L. I. Zane, Rev. Mod. Phys. **43**, 532 (1971); M. G. Richards, J. Pope, P. S. Tofts, and J. H. Smith, J. Low Temp. Phys. **24**, 1 (1976); M. G. Richards, J. H. Smith, P. S. Tofts, and W. J. Mullin, Phys. Rev. Lett. **34**, 1545 (1975); V. A. Mikheev, V. A. Maidanov, and N. P. Mikhin, Solid State Commun. **48**, 361 (1983); A. R. Allen, M. G. Richards, and J. Schratter, J. Low Temp. Phys. **47**, 289 (1982).
[23] J. G. Dash, *Films on Solid Surfaces* (Academic, New York, 1975); M. Schick, in *Phase Transitions in Surface Films*, edited by J. G. Dash and J. Ruvalds (Plenum, New York, 1980); L. W. Bruch, M. W. Cole, and E. Zaremba, *Physical Adsorption: Forces and Phenomena* (Oxford, New York, 1997).
[24] M. C. Gordillo and D. M. Ceperley, Phys. Rev. B **58**, 6447 (1998).
[25] M. Pierce and E. Manousakis, Phys. Rev. B **62**, 5228 (2000).
[26] J. E. Cuervo, P.-N. Roy, and M. Boninsegni, J. Chem. Phys. **122**, 114504 (2005).
[27] R. A. Aziz, V. P. S. Nain, J. S. Carley, W. L. Taylor, and G. T. McConville, J. Chem. Phys. **70**, 4330 (1979).
[28] M. Boninsegni and D. M. Ceperley, Phys. Rev. Lett. **74**, 2288 (1995).
[29] D. E. Galli, M. Rossi, and L. Reatto, Phys. Rev. B **71**, 140506(R) (2005).
[30] M. Pierce and E. Manousakis, Phys. Rev. Lett. **81**, 156 (1998); Phys. Rev. B **59**, 3802 (1999); Phys. Rev. Lett. **83**, 5314 (1999); Phys. Rev. B **63**, 144524 (2001).
[31] E. Manousakis, V. R. Pandharipande, and Q. N. Usmani, Phys. Rev. B **31**, 7022 (1985).